Long-range antiferromagnetic order in the frustrated *XY* pyrochlore antiferromagnet $Er_2Ge_2O_7$

X. Li,[1] W. M. Li,[1] K. Matsubayashi,[2] Y. Sato,[3] C. Q. Jin,[1] Y. Uwatoko,[2] T. Kawae,[3] A. M. Hallas,[4] C. R. Wiebe,[4,5] A. M. Arevalo-Lopez,[6] J. P. Attfield,[6] J. S. Gardner,[7] R. S. Freitas,[8] H. D. Zhou,[9] and J.-G. Cheng[1,2,*]

[1]*Beijing National Laboratory for Condensed Matter Physics and Institute of Physics, Chinese Academy of Sciences, Beijing 100190, China*

[2]*Institute for Solid State Physics, University of Tokyo, 5-1-5 Kashiwanoha, Kashiwa, Chiba 277-8581, Japan*

[3]*Department of Applied Quantum Physics, Faculty of Engineering, Kyushu University, Fukuoka, 819-0395, Japan*

[4]*Department of Physics and Astronomy, McMaster University, 1280 Main St. W, Hamilton, ON, Canada, L8S 4M1*

[5]*Department of Chemistry, University of Winnipeg, Winnipeg, Manitoba, Canada, R3B 2E9*

[6]*Centre for Science at Extreme Conditions and School of Chemistry, University of Edinburgh, King's Buildings, Mayfield Road, Edinburgh EH9 3JZ, United Kingdom*

[7]*National Synchrotron Radiation Research Center, Neutron Group, Hsinchu 30077, Taiwan*

[8]*Instituto de Física, Universidade de São Paulo, C. P. 66318-05314-970 São Paulo, SP. Brazil*

[9]*Department of Physics and Astronomy, University of Tennessee, Knoxville, Tennessee, 37996, USA*

(Received 11 November 2013; revised manuscript received 17 January 2014; published 12 February 2014)

A cubic $Er_2Ge_2O_7$ pyrochlore was prepared under high-pressure and high-temperature conditions and its magnetic ground state was investigated by measurements of specific heat, dc and ac magnetic susceptibility as functions of temperature, pressure, and magnetic field. We found that $Er_2Ge_2O_7$ undergoes a long-range antiferromagnetic transition at $T_N \approx 1.4$ K, which can be further enhanced by applying external physical pressure. On the other hand, application of external magnetic fields suppresses the antiferromagnetic order to zero temperature around $H_c \approx 2.3$ T, where a magnetic-field-induced spin-flop transition was observed. H_c increases accordingly with increasing T_N under external pressure. A comparison of the magnetic ground states and structural variations along the isostructural series $Er_2B_2O_7$ (B = Sn, Ti, Ge) together with the high-pressure study on $Er_2Ge_2O_7$ indicated that the magnetic properties of these highly frustrated *XY* pyrochlore antiferromagnets are very sensitive to the minute structural changes that determine the anisotropic exchange interactions and the local crystal-electric-field environments of Er^{3+} ions.

DOI: 10.1103/PhysRevB.89.064409 PACS number(s): 75.30.Kz, 75.40.−s, 75.30.−m

Recently, much attention has been paid to the pyrochlore compound $Er_2Ti_2O_7$, which has been regarded as a promising textbook example where the exotic "order-by-disorder" (OBD) mechanism plays a decisive role in selecting the long-range-ordered ground state [1–7]. In $Er_2Ti_2O_7$, the Er^{3+} ions form a three-dimensional network of corner-sharing tetrahedra, i.e., the so-called pyrochlore lattice, and exhibit strong easy-plane anisotropy with local moments confined to planes orthogonal to the local ⟨111⟩ axis of tetrahedron [2]. These facts make $Er_2Ti_2O_7$ an ideal experimental realization of a highly frustrated *XY* antiferromagnet on the pyrochlore lattice [2,8]. Earlier numerical simulations on the classical ⟨111⟩ *XY* pyrochlore antiferromagnet found a macroscopic degeneracy of the magnetic ground state, which can be lifted by finite-temperature thermal fluctuations, leading the system to a $\mathbf{q} = 0$ conventional Néel state via the OBD mechanism [1]. This prediction was later confirmed experimentally in $Er_2Ti_2O_7$, which was found to develop a long-range antiferromagnetic order below $T_N = 1.173$ K [2]. In sharp contrast to the prediction of a coplanar ψ_3 state, however, the spin ordered state under zero field can be described almost entirely with a noncoplanar ψ_2 structure [2,9]. This discrepancy has left the OBD effect as the most favorable selection mechanism for the experimentally observed noncoplanar ψ_2 ground state. Such an OBD scenario was further reinforced by more recent theoretical investigations based on an effective pseudo-spin-1/2 Hamiltonian with anisotropic exchange interactions [4,5]. By varying the relative magnitude of these anisotropic exchange couplings $J_{ex} \equiv \{J_{\pm}, J_{\pm\pm}, J_{z\pm}, J_{zz}\}$, Wong *et al.* [6] further presented comprehensive ground-state phase diagrams of *XY* pyrochlore magnets, which were found to be very sensitive to the minute changes of J_{ex}.

Despite these significant achievements in understanding the magnetically ordered state of $Er_2Ti_2O_7$, it remains elusive why the isostructural $Er_2Sn_2O_7$ with a nearly identical Er^{3+} pyrochlore lattice does not form a long-range-ordered state down to 100 mK [10–13]. A very recent neutron study on $Er_2Sn_2O_7$ revealed the existence of short-range correlations, in which the magnetic moments are arranged in the Palmer-Chalker configurations favored by the dipolar interactions [12,14]. A comparison of the crystal-electric-field (CEF) and the anisotropic exchange parameters between $Er_2Sn_2O_7$ and $Er_2Ti_2O_7$ indicated that the former compound has a stronger planar character of Er^{3+} moment, but less anisotropic exchange couplings [12]. Variations of these microscopic parameters that influence the ground states of $Er_2B_2O_7$ (B = Ti, Sn) should have a deep root on the minor structural changes in these closely related compounds. An intuitive expectation would connect with their different nearest-neighbor distance R_{nn} between Er^{3+} ions. Therefore, a systematic study on the magnetic ground states of $Er_2B_2O_7$ by spanning R_{nn} to a large extent is indispensable in order to achieve a thorough understanding.

For this purpose, we have chosen to replace Ti^{4+} (0.605 Å) and Sn^{4+} (0.69 Å) with the much smaller Ge^{4+} ion (0.53 Å) so as to exert a larger chemical pressure on the Er^{3+} pyrochlore lattice. As reported earlier [15], high-pressure and

*jgcheng@iphy.ac.cn

 ©2014 American Physical Society

high-temperature (HPHT) synthesis is required in order to stabilize the cubic pyrochlore structure for $Er_2Ge_2O_7$. In this paper, we report on the HPHT synthesis and the structural analysis of the cubic pyrochlore $Er_2Ge_2O_7$, followed by detailed characterizations on the low-temperature magnetic properties of this *XY* pyrochlore antiferromagnet. As expected, the application of chemical pressure results in a global, uniform reduction of lattice dimension or R_{nn}. Structural refinement on $Er_2Ge_2O_7$ enables one to see subtle modifications of the local CEF environments of Er^{3+} ions along the series $Er_2B_2O_7$ (B = Sn, Ti, Ge). Measurements of low-temperature specific heat and dc magnetic susceptibility revealed that like $Er_2Ti_2O_7$ [2], $Er_2Ge_2O_7$ also develops a long-range antiferromagnetic order below $T_N \approx 1.40$ K, which is higher than the reported $T_N = 1.173$ K of $Er_2Ti_2O_7$. In addition, we found that T_N of $Er_2Ge_2O_7$ can be further enhanced by applying external physical pressure, but T_N tends to saturate with pressure. These results indicate that the magnetic ground state of *XY* pyrochlore antiferromagnets $Er_2B_2O_7$ is very sensitive to structural changes. Furthermore, measurements of dc and ac magnetic susceptibility under different dc magnetic fields H_{dc} revealed the existence of quantum critical point around $H_c \approx 2.3$ T, where the long-range ordered state gives way to a highly polarized state. The critical magnetic field H_c was found to increase slightly with increasing T_N under pressure.

The cubic $Er_2Ge_2O_7$ pyrochlore in the present study was prepared under 7 GPa and 1000 °C by using a Walker-type multianvil module (Rockland Research Co.) in the Institute of Physics, Chinese Academy of Sciences. Another $Er_2Ge_2O_7$ sample obtained under 8 GPa and 1100 °C at the University of Edinburgh shows similar results (not shown here). Phase purity of the obtained high-pressure products was examined by powder x-ray diffraction (XRD) at room temperature. Direct current magnetization was measured with a commercial Superconducting Quantum Interference Device (SQUID) magnetometer (Quantum Design) equipped with a home-made ^{3}He insert [16]. Specific-heat data in the temperature range 0.5–30 K were collected by using a ^{3}He option of the Physical Property Measurement System (PPMS, Quantum Design). Alternating current magnetic susceptibility under pressures up to ~20 kbar was measured by employing a primary-secondary-coil technique inside a self-clamped piston-cylinder cell, which was attached to commercial Heliox insert (Oxford Instruments). An excitation current of about 2 mA with a frequency of 317 Hz was applied to the primary coil during the measurements. The pressure inside the high-pressure cell was monitored by measuring the superconducting transition temperature of lead (Pb). Glycerin was used as the pressure transmitting medium.

The powder XRD pattern shown in Fig. 1(a) confirmed that the as-obtained $Er_2Ge_2O_7$ sample is single phase with the cubic pyrochlore structure. To extract more structural information, we have refined the XRD pattern in a cubic *Fd-3m* (No. 227) space group with the Er atom at 16*d* (1/2, 1/2, 1/2), the Ge atom at 16*c* (0, 0, 0,), the O1 atom at 48*f* (x, 1/8, 1/8), and the O2 atom at 8*b* (3/8, 3/8, 3/8) site, respectively. The structural parameters after refinements are given in Table I together with those of $Er_2Ti_2O_7$ (Ref. [17]) and $Er_2Sn_2O_7$ (Ref. [18]) for comparison. The obtained lattice parameter $a = 9.8782(2)$ Å is consistent with the

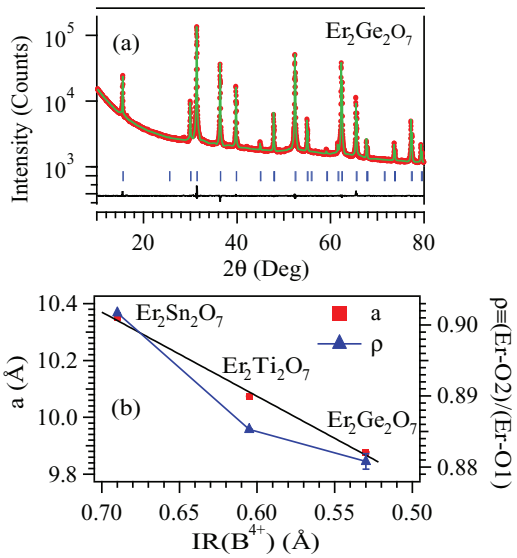

FIG. 1. (Color online) (a) Powder XRD pattern of $Er_2Ge_2O_7$ after Rietveld refinement. (b) Lattice parameter a and the Er-O bond-length ratio $\rho \equiv$(Er-O2)/(Er-O1) characterizing the axial distortion of ErO_8 polyhedra in the series of $Er_2B_2O_7$ (B = Sn, Ti, Ge) as a function of ionic radius (IR) of B^{4+} ions.

value reported previously [15], and is much smaller than that of $Er_2Ti_2O_7$ (a = 10.074 Å) [17] and $Er_2Sn_2O_7$ (a = 10.35 Å) [18]. As shown in Fig. 1(b) and Table I, with decreasing the ionic radius (IR) of B^{4+} ions along the $Er_2B_2O_7$ series, the cubic lattice parameter a and the corresponding R_{nn} [$\equiv(\sqrt{2}/4)a$] decrease linearly, signaling a progressive increment of chemical pressure on the Er^{3+} pyrochlore lattice by reducing the B^{4+}-ion size.

In addition to the global, uniform reduction of lattice dimension upon the application of chemical pressure along the $Er_2B_2O_7$ series, the local coordination around Er^{3+} ions also experiences subtle modifications, which should have a nontrivial impact on the CEF and in turn on the anisotropic magnetic degree of freedom of Er^{3+} ions. In the $Er_2B_2O_7$ pyrochlores, the Er atoms are coordinated by six O1 and two O2 atoms; the much shorter Er-O2 bonds produce a pronounced axial distortion along the local ⟨111⟩ direction. In general, this distortion increases with decreasing x [8], which is indeed observed along this series $Er_2B_2O_7$ (B = Sn, Ti, Ge). As shown in Table I, however, variation of x

TABLE I. Comparison on the structural parameters of cubic pyrochlores $Er_2B_2O_7$ (B = Ge, Ti, Sn).

$Er_2B_2O_7$	B = Ge	B = Ti	B = Sn
IR(B^{4+}) (Å)	0.53	0.605	0.69
a (Å)	9.8782(2)	10.074(1)	10.3504(1)
R_{nn} [$\equiv(\sqrt{2}/4)a$] (Å)	3.492	3.562	3.659
x of O1at 48*f* (x, 1/8, 1/8)	0.3292(6)	0.331	0.3375
Er-O2 (×2) (Å)	2.1387(1)	2.1811	2.2409
Er-O1 (×6) (Å)	2.428(3)	2.4637	2.4853
ρ [≡(Er-O2)/(Er-O1)]	0.881(1)	0.8853	0.9017
Reference	this work	[17]	[18]

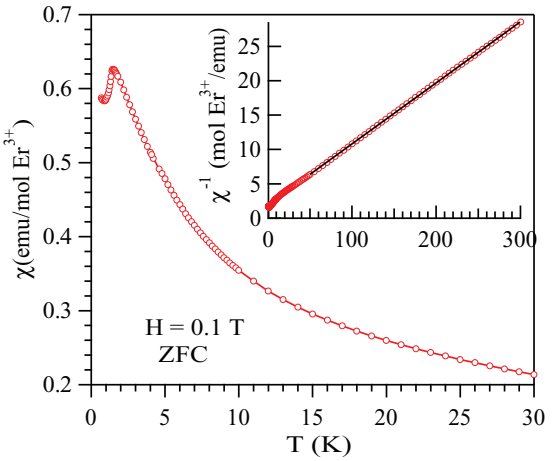

FIG. 2. (Color online) Temperature dependence of the dc magnetic susceptibility $\chi(T)$ of $Er_2Ge_2O_7$ measured under $H = 0.1$ T in zero-field-cooling (ZFC) mode. Inset shows the inverse susceptibility $\chi^{-1}(T)$ in the whole temperature range and the Curie-Weiss fitting curve between 50 and 300 K.

values as a function of IR is not uniform: Δx/IR is 0.076/Å from $Er_2Sn_2O_7$ to $Er_2Ti_2O_7$, but it is only 0.024/Å from $Er_2Ti_2O_7$ to $Er_2Ge_2O_7$. Here, we introduce an Er-O bond-length ratio $\rho \equiv$ (Er-O2)/(Er-O1) to further characterize this axial distortion; the smaller ρ, the stronger axial distortion. As seen in Fig. 1(b), with reducing IR(B^{4+}) in this series, ρ does not decrease linearly as the lattice constant a does, but tends to level off, which implies that the local CEF environments might change only slightly with further applying chemical or physical pressure. It is worth noting that ρ scales linearly with x.

The availability of $Er_2Ge_2O_7$ enables us to check the magnetic ground state of XY pyrochlore antiferromagnet with a much reduced lattice dimension and a stronger local structural distortion. The main panel of Fig. 2 displays the temperature dependence of the dc magnetic susceptibility $\chi(T)$ of $Er_2Ge_2O_7$ between 0.7 and 30 K measured under $H =$ 0.1 T after zero-field cooling (ZFC) from room temperature. A cusplike anomaly at about 1.4 K was clearly observed, signaling the appearance of long-range antiferromagnetic ordering. The inverse magnetic susceptibility $\chi^{-1}(T)$ shown in the inset of Fig. 2 follows nicely the Curie-Weiss (CW) behavior in the paramagnetic region; a CW fitting to $\chi^{-1}(T)$ in the temperature range 50–300 K yields an effective moment $\mu_{\rm eff} = 9.50(1)\ \mu_B/Er^{3+}$ and a Weiss temperature $\theta_{\rm CW} = -21.9(2)$ K. The obtained $\mu_{\rm eff}$ is close to that of $Er_2Sn_2O_7$ [11,12] and $Er_2Ti_2O_7$ [19], and is in excellent agreement with the expected value of 9.58 μ_B for the $^4I_{15/2}$ ground state of Er^{3+}. In comparison with the $\theta_{\rm CW}$ values of -14.32 K for $Er_2Sn_2O_7$ [11,12] and -15.93 K for $Er_2Ti_2O_7$ [19], the larger $|\theta_{\rm CW}|$ of $Er_2Ge_2O_7$ should be attributed to the enhanced CEF effect.

Figure 3(a) shows the temperature dependence of specific heat $C(T)$ of $Er_2Ge_2O_7$ measured between 0.5 and 30 K under zero magnetic field. As can be seen, $C(T)$ exhibits a sharp peak at $T_N = 1.41$ K, in excellent accordance with the χ(T) anomaly shown in Fig. 2, further confirming a second-order

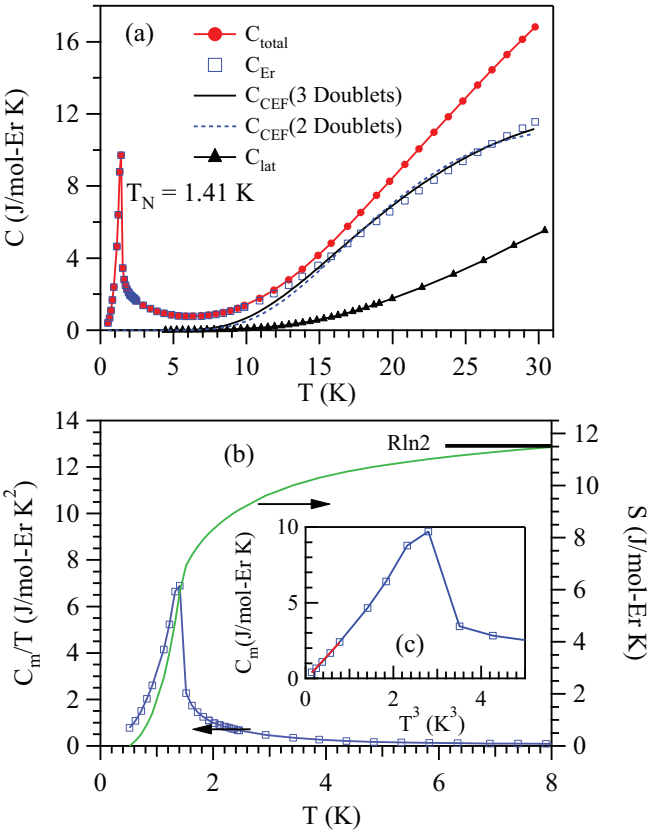

FIG. 3. (Color online) (a) Temperature dependence of specific heat $C(T)$ of $Er_2Ge_2O_7$. See the text for the analysis. (b) Magnetic specific heat C_m and entropy S associated with the long-range antiferromagnetic transition. (c) A plot of C_m vs T^3. The solid line is a linear fitting curve.

phase transition to an antiferromagnetically ordered state below T_N.

In order to extract the magnetic contribution C_m and to estimate the entropy associated with this transition, we measured $C(T)$ of an isostructural, nonmagnetic $Lu_2Ge_2O_7$ pyrochlore as the lattice standard $C_{\rm lat}$. After subtracting $C_{\rm lat}$ from the measured $C_{\rm total}$, we obtained the specific-heat contribution from the magnetic Er^{3+} ions, $C_{\rm Er}$. As shown in Fig. 3(a), besides the low-temperature peak, there exists a substantial contribution above 10 K associated with the Er^{3+} CEF levels, $C_{\rm CEF}$. As the 16-fold degeneracy of Er^{3+} ($J = 15/2$) is expected to split into eight doublets in the D_{3d} symmetry, we have tried to simulate the $C_{\rm CEF}$ by considering the first two doublets (two doublets) or the first three doublets (three doublets), respectively. As can be seen, the latter gives a better description to $C_{\rm Er}$ between 15 and 30 K, but both underestimate the measured $C(T)$ below 15 K. From the best fitting, the first and second excited doublets are found to be located at 73(6) K and 150(70) K, respectively. The large uncertainty of the second excited doublet arises from the limited fitting range, but the estimated value for the first excited doublet, ~6.3 meV, agrees in general with that of $Er_2Ti_2O_7$ and $Er_2Sn_2O_7$ determined from neutron scattering measurements [2,12,13].

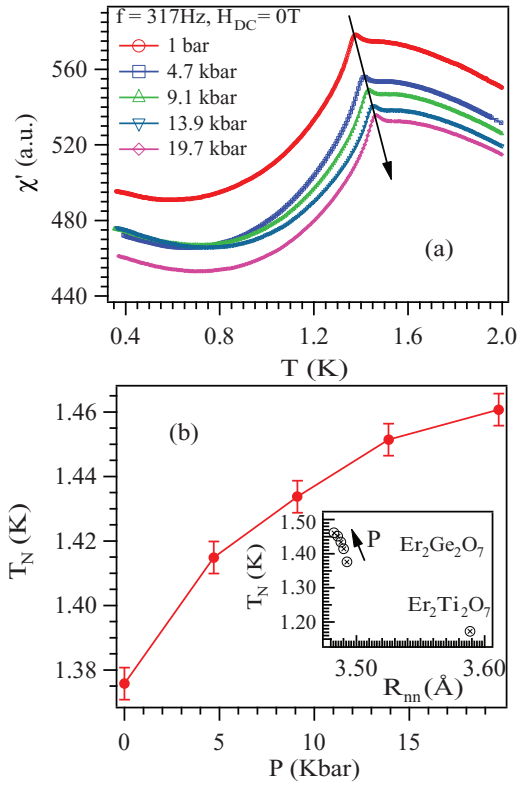

FIG. 4. (Color online) (a) Temperature dependence of the zero-field ac magnetic susceptibility $\chi'(T)$ measured under different external pressures up to 19.7 kbar for $Er_2Ge_2O_7$. (b) Pressure dependence of T_N determined from the maximum of $\chi'(T)$ in (a). The obtained T_N is replotted in the inset as a function of R_{nn} based on the bulk modulus of $B_0 = 228$ GPa for $Er_2Ge_2O_7$. The ambient-pressure data of $Er_2Ti_2O_7$ is also included for comparison.

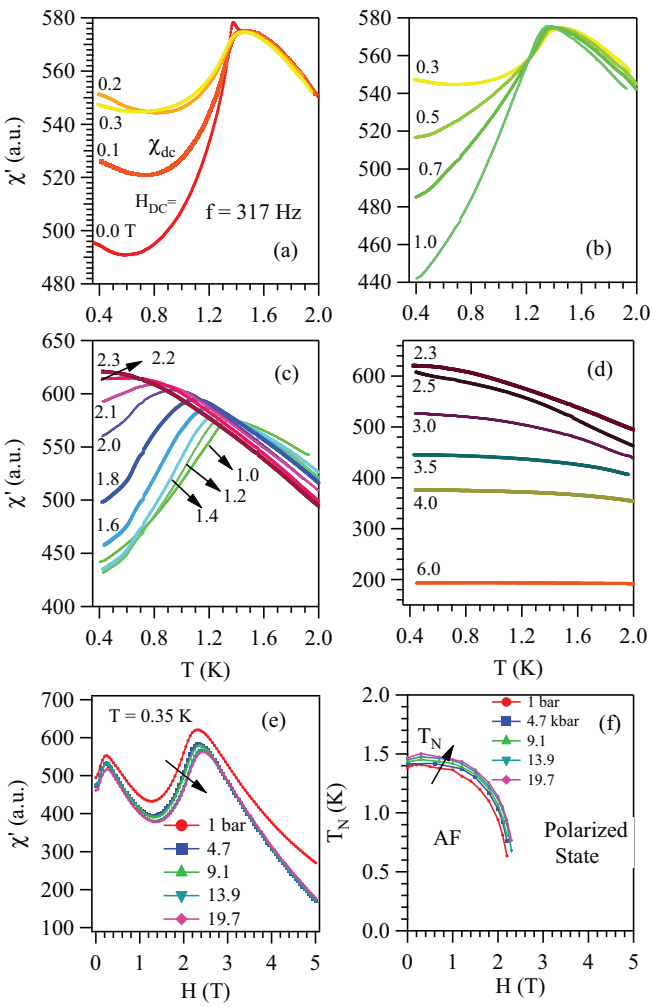

FIG. 5. (Color online) (a)–(d) Temperature dependence of the ambient-pressure $\chi'(T)$ under different magnetic fields up to 6 T. (e) Field dependence of $\chi'(H)$ measured at $T = 0.35$ K under different pressures. (f) Field dependence of $T_N(H)$ under different pressures.

Finally, C_m is obtained by $C_m = C_{\text{total}} - C_{\text{lat}} - C_{\text{CEF}}$, and is shown in Fig. 3(b). The magnetic entropy S obtained by integrating C_m/T almost saturates to its ideal value of $R\ln(2S+1)$ with $S = 1/2$. This points to the effective $S = 1/2$ pseudo-spin character of the magnetic Er^{3+} ions with a Kramers doublet ground state [20]. In addition, greater than 50% of the entropy is found to release above T_N, suggesting the existence of profound short-range spin correlations before finally establishing the long-range order. On the other hand, C_m below T_N follows nicely the T^3 dependence at least up to 1.1 K, as shown in Fig. 3(c). A linear fitting to $C_m = \sigma T^3$ yields a coefficient $\sigma = 3.14$ J/(mol Er K^4). Similar behavior has also been observed in $Er_2Ti_2O_7$ [2,20].

The observation of a higher $T_N = 1.4$ K in $Er_2Ge_2O_7$ than that of 1.17 K in $Er_2Ti_2O_7$ indicated that the chemical pressure applied on the Er^{3+} pyrochlore lattice can promote the long-range antiferromagnetic ordering. This finding motivated us to check if the T_N of $Er_2Ge_2O_7$ can be further enhanced by applying external physical pressure. Figure 4 displays the ac magnetic susceptibility $\chi'(T)$ of $Er_2Ge_2O_7$ measured below 2 K under zero magnetic field in the presence of different pressures up to 19.7 kbar. As can be seen, the overall feature of $\chi'(T)$ resembles that of dc $\chi(T)$ data shown in Fig. 2. We defined T_N as the maximum of $\chi'(T)$. At ambient pressure, the measured $T_N = 1.376$ K agrees well with that determined from $\chi(T)$ and $C(T)$. With increasing pressure, T_N shifts gradually to higher temperatures and reaches 1.461 K at 19.7 kbar. The pressure dependence of $T_N(P)$ is shown in the main panel of Fig. 4(b). As can be seen, T_N does not increase linearly with pressure, but seems to saturate with further applying pressure. Thus, the combined chemical and physical pressure study indicated that the long-range antiferromagnetic transition temperature is sensitive to structural changes, but exhibits a complex behavior. We will return to this point below.

We further explored the stability of the long-range antiferromagnetic order under external magnetic fields at each pressure. Figures 5(a)–5(d) present the ambient-pressure ac $\chi'(T)$ data of $Er_2Ge_2O_7$ under different magnetic fields H_{dc} up to 6 T. As can be seen in Fig. 5(a), the $\chi'(T)$ under $H_{dc} = 0.1$ T resembles the dc $\chi(T)$ curve shown in Fig. 2, showing a relatively broad cusplike anomaly around $T_N = 1.4$ K followed by a low-temperature upturn. This comparison thus confirms our ac susceptibility data obtained by using a home-made primary-secondary coil. The small peaklike feature in the zero-field $\chi'(T)$ curve smears out immediately upon the application of external fields. With increasing H_{dc}, the evolution of $\chi'(T)$

can be divided into four regions: (1) for $0 \leq H_{dc} \leq 0.2$ T, T_N remains essentially constant; $\chi'(T)$ is nearly unchanged for $T > T_N$, but is enhanced dramatically for $T < T_N$; (2) for $0.3 \leq H_{dc} \leq 1.0$ T, T_N decreases slightly and the low-temperature upturn in $\chi'(T)$ is suppressed gradually; (3) for $1.0 \leq H_{dc} \leq 2.3$ T, the cusplike anomaly of $\chi'(T)$ at T_N transforms to a broad maximum, which shifts progressively to lower temperatures with increasing H_{dc} and completely disappears around 2.3 T; (4) for $2.3 < H_{dc} \leq 6.0$ T, no anomaly can be discerned in $\chi'(T)$ and the magnitude of $\chi'(T)$ in the measured temperature region drops quickly. Similar features were observed for $\chi'(T)$ data under different high pressures. The evolution of $\chi'(T)$ in these four regions can be tracked by monitoring the field dependence of $\chi'(H)$ measured at $T = 0.35$ K, the lowest temperature of our present study. As shown in Fig. 5(e), $\chi'(H)$ curves at different pressures all exhibit a double-peak structure: the first peak corresponds to the initial enhancement of $\chi'(T)$ below T_N under low H_{dc}, and the second peak to the critical magnetic field H_c where T_N is suppressed to below 0.35 K. As can be seen, upon application of external pressure, the first peak does not exhibit noticeable change, whereas the second peak moves gradually to higher temperatures, consistent with the enhancement of H_c with pressure. Finally, the field dependencies of $T_N(H)$ determined from $\chi'(T, H_{dc})$ curves at different pressures are summarized in Fig. 5(f). It is clear that both T_N and H_c increases with pressure. These results demonstrated that, on the one hand, the application of external magnetic field destabilizes the long-range antiferromagnetic order, leading to a zero-temperature quantum critical point around $H_c = 2.3$ T at ambient pressure, and on the other hand, the application of physical pressure stabilizes the long-range antiferromagnetic order, leading to an enhancement of both T_N and H_c.

In order to gain insights into the high-field phase above H_c, we turn to the temperature and field dependence of dc magnetization. As shown in Fig. 6(a), the dc $\chi(T)$ data under different magnetic fields resemble those of ac $\chi'(T)$ data shown in Figs. 5(a)–5(d). The $\chi(T)$ curve measured under $H = 4$ T $> H_c$ exhibits a ferromagnetic like saturation behavior, which suggested that the sample enters a highly

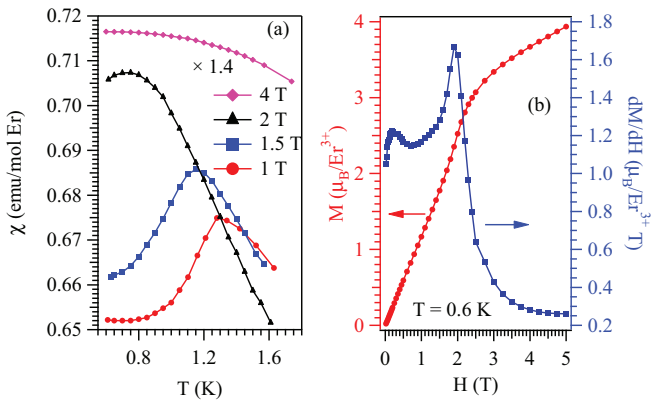

FIG. 6. (Color online) (a) Temperature dependence of the dc magnetic susceptibility $\chi(T)$ under different magnetic fields up to 4 T. (b) Magnetization curve $M(H)$ and its derivative dM/dH measured at $T = 0.6$ K.

polarized state under $H > H_c$. This is confirmed by the $M(H)$ measurement below T_N. As shown in Fig. 6(b), the $M(H)$ curve measured at $T = 0.6$ K displays a clear slope change around $H_c = 2.3$ T, which corresponds to a sharp peak in the dM/dH curve and signals a field-induced spin-flop transition from an antiferromagnetic state for $H < H_c$ to a highly polarized state for $H > H_c$. The weak peak located around 0.2 T in both dM/dH and $\chi'(H)$ curves might be associated with the alignment of magnetic domains.

Our detailed characterizations on the cubic $Er_2Ge_2O_7$ pyrochlore thus confirm that it develops into long-range antiferromagnetic order below $T_N \approx 1.4$ K, with several similar characteristics as its sister compound, $Er_2Ti_2O_7$, as detailed below: (1) the λ-shaped specific-heat anomaly around T_N evidences a continuous, second-order phase transition; (2) the magnetic specific heat follows the $C_m \propto T^3$ dependence below T_N; (3) the magnetic entropy saturates to the expected value of $R\ln 2$ for $S = ½$; (4) a quantum critical point (QCP) can be reached by suppressing the T_N smoothly to zero temperature via the application of external magnetic fields. It has been well known that the first two observations contradict classical theories [2], which predicted a first-order transition with a constant density of low-lying excitations. Very recent studies have achieved significant progress on this problem. Zhitomirsky *et al.* [4] calculated the low-energy excitation spectrum of $Er_2Ti_2O_7$ based on an effective "pseudodipolar" spin-1/2 model, and found a gapless mode with linear dispersion, which can account for the experimentally observed $C_m = \sigma T^3$ dependence as well as the inelastic neutron spectrum. Savary *et al.* [5] proposed that the slope σ is related to the mean spin-wave velocity $\bar{v}$ of the pseudo-Goldstone mode, i.e., $\sigma = k_B^4 \pi^2 a^3 / 120 \bar{v}^3$. By using the experimental values of $\sigma(\ Er_2Ge_2O_7) = 3.14$ J/(mol Er K^4) obtained in the present study and the $\sigma(\ Er_2Ti_2O_7) = 4.6$ J/(mol Er K^4) [5], as well as the lattice constants shown in Table I, we can estimate that $\bar{v}$ of $Er_2Ge_2O_7$ is about 1.11 times that of $Er_2Ti_2O_7$, roughly consistent with the ratio of T_N, i.e., 1.19, since the velocity $\bar{v}$ is roughly proportional to the overall exchange interactions (see Supplemental Material of Ref. [5]). Based on an effective pseudo-spin-1/2 Hamiltonian with anisotropic exchange interactions, the experimentally observed noncoplanar ψ_2 state for $Er_2Ti_2O_7$ has recently been confirmed to be selected by the quantum fluctuations via the OBD mechanism [4–6]. The importance of quantum fluctuations is consistent with the observation (3), which points to an effective $S = 1/2$ pseudo-spin character of the ground state Kramers doublet of Er^{3+} ions. By means of single-crystal neutron scattering measurements, Ruff *et al.* [3] have shown explicitly that the magnetic-field-induced QCP in $Er_2Ti_2O_7$ corresponds to a smooth transformation from the noncoplanar ψ_2 structure to a highly polarized *XY* state. Although neutron scattering measurements are needed to determine if $Er_2Ge_2O_7$ adopts a similar magnetic structure as $Er_2Ti_2O_7$, our magnetization curves shown in Fig. 6 as well as the field-induced QCP [3] suggest that a similar process should take place in both compounds.

The availability of $Er_2Ge_2O_7$ offers us an excellent opportunity to look into the critical factors governing the magnetic ground state of the $Er_2B_2O_7$ series, a family of *XY* pyrochlore antiferromagnets. As mentioned earlier, although short-range

correlations with the Palmer-Chalker configurations have been detected in $Er_2Sn_2O_7$, [11,12] it does not show any long-range order down to 100 mK. In contrast, $Er_2Ti_2O_7$ undergoes an antiferromagnetic transition at $T_N = 1.173$ K [2]. The observed higher T_N in $Er_2Ge_2O_7$ clearly indicated that the application of chemical pressure plays an important role in determining the magnetic ground state. This conclusion is further supported by our high-pressure $\chi'(T)$ results shown in Fig. 4, where the application of physical pressure can further enhance T_N of $Er_2Ge_2O_7$. This is understandable since the strength of exchange interactions J_{ex} including the nearest- and the next-nearest-neighbor ones should be reinforced dramatically with decreasing R_{nn}. Earlier numerical calculations by Bramwell *et al.* [1] have predicted that the long-range order of *XY* pyrochlore antiferromagnets takes place at $T_N \sim 0.1\ J_{ex}$. Recent investigations have realized the importance of anisotropic exchange interactions for the *XY* pyrochlore antiferromagnets; the ground-state phase diagrams were found to be very sensitive to the minute change of the relative magnitude of these anisotropic exchange couplings $J_{ex} \equiv \{J_{\pm}, J_{\pm\pm}, J_{z\pm}, J_{zz}\}$ [6,7]. As shown in Fig. 1(b), the effect of chemical pressure applied on the Er^{3+} pyrochlore lattice via reducing the IR of B^{4+} ions is at least twofold: (1) a global, uniform reduction of lattice dimension that reduces the nearest-neighbor Er^{3+} distance R_{nn} and (2) a strengthening of the local axial distortion of ErO_8 polyhedron that can change the local CEF environment of Er^{3+} ions. Both factors are expected to change effectively the relative magnitude of these four independent anisotropic exchange couplings J_{ex}, and thus T_N.

Although our combined chemical and physical pressure studies demonstrated unambiguously an intimate correlation between T_N and structural changes, we cannot reach a simple relationship between T_N and R_{nn}. By using a bulk modulus $B_0 = 228$ (4) GPa determined from our high-pressure XRD measurements on $Er_2Ge_2O_7$, we have determined $R_{nn}(P)$ and plotted the T_N of $Er_2Ge_2O_7$ as a function of R_{nn} in the inset of Fig. 4(b). As can be seen, the ambient-pressure data of $Er_2Ti_2O_7$ does not fall on the extrapolated curve of $T_N(R_{nn})$ of $Er_2Ge_2O_7$. This observation indicated that in addition to R_{nn}, the subtle changes of local CEF environment also influence dramatically J_{ex} and T_N. Although the resolution of our high-pressure XRD does not allow us to extract reliable information regarding the local distortion, the observations that both the Er-O bond-length ratio $\rho \equiv$ (Er-O2)/(Er-O1) in Fig. 1(b) and $T_N(P)$ in Fig. 4(b) tend to saturate with reducing R_{nn} imply an important correlation between T_N and the local distortions of Er^{3+} ions. To gain a better understanding, future studies on the solid solutions of $Er_2(Ge_{1-x}Ti_x)_2O_7$ are planned with a focus on the detailed evolutions of T_N and local structural changes.

In summary, we have prepared the cubic $Er_2Ge_2O_7$ pyrochlore under 7 GPa and 1000 °C and characterized in details its magnetic ground state by measuring low-temperature specific heat, dc and ac magnetic susceptibility under external pressure and magnetic fields. We found that $Er_2Ge_2O_7$ forms a long-range antiferromagnetic order below $T_N \approx 1.4$ K, with similar characteristics as the well-studied $Er_2Ti_2O_7$. The application of external magnetic fields suppresses the antiferromagnetic order continuously to zero temperature and leads to a highly polarized state above $H_c \approx 2.3$ T. On the other hand, the application of physical pressure can stabilize antiferromagnetic order, leading to higher T_N and H_c. Neutron scattering experiments are planned to determine the magnetic structure and excitations of this *XY* pyrochlore antiferromagnet.

ACKNOWLEDGMENTS

Work at IOP, CAS is supported by the NSFC, MOST, and Chinese Academy of Sciences (Grant Nos. 11304371, 2014CB921500, and Y2K5016 × 51). Work at ISSP, University of Tokyo was partially supported by Grant-in-Aid for Scientific Research, KAKENHI (Grant Nos. 12F02023, 24740220, 23340101, and 252460135). C.R.W. acknowledges support from NSERC, the CRC program, CFI, and the ACS petroleum Fund. J.P.A. acknowledges support from EPSRC and the Royal Society.

[1] S. T. Bramwell, M. J. P. Gingras, and J. N. Reimers, J. Appl. Phys. **75**, 5523 (1994).
[2] J. D. M. Champion, M. J. Harris, P. C. W. Holdsworth, A. S. Wills, G. Balakrishnan, S. T. Bramwell, E. Čižmár, T. Fennell, J. S. Gardner, J. Lago, D. F. McMorrow, M. Orendáč, A. Orendáčová, D. McK. Paul, R. I. Smith, M. T. F. Telling, and A. Wildes, Phys. Rev. B **68**, 020401(R) (2003).
[3] J. P. C. Ruff, J. P. Clancy, A. Bourque, M. A. White, M. Ramazanoglu, J. S. Gardner, Y. Qiu, J. R. D. Copley, M. B. Johnson, H. A. Dabkowska, and B. D. Gaulin, Phys. Rev. Lett. **101**, 147205 (2008).
[4] M. E. Zhitomirsky, M. V. Gvozdikova, P. C. W. Holdsworth, and R. Moessner, Phys. Rev. Lett. **109**, 077204 (2012).
[5] L. Savary, K. A. Ross, B. D. Gaulin, J. P. C. Ruff, and L. Balents, Phys. Rev. Lett. **109**, 167201 (2012).
[6] A. W. C. Wong, Z. Hao, and M. J. P. Gingras, Phys. Rev. B **88**, 144402 (2013).
[7] H. Yan, O. Benton, L. Jaubert, and N. Shannon, arXiv:1311.3501v1.
[8] J. S. Gardner, M. J. P. Gingras, and J. E. Greedan, Rev. Mod. Phys. **82**, 53 (2010).
[9] A. Poole, A. S. Wills, and E. Lelièvre-Berna, J. Phys.: Condens. Matter **19**, 452201 (2007).
[10] J. Lago, T. Lancaster, S. J. Blundell, S. T. Bramwell, F. L. Pratt, M. Shirai, and C. Baines, J. Phys.: Condens. Matter **17**, 979 (2005).
[11] K. Matsuhira, Y. Hinatsu, K. Tenya, H. Amitsuka, and T. Sakakibara, J. Phys. Soc. Jpn. **71**, 1576 (2002).
[12] P. M. Sarte, H. J. Silverstein, B. T. K. Van Wyk, J. S. Gardner, Y. Qiu, H. D. Zhou, and C. R. Wiebe, J. Phys.: Condens. Matter **23**, 382201 (2011).
[13] S. Guitteny, S. Petit, E. Lhotel, J. Robert, P. Bonville, A. Forget, and I. Mirebeau, Phys. Rev. B **88**, 134408 (2013).
[14] S. E. Palmer and J. T. Chalker, Phys. Rev. B **62**, 488 (2000).

[15] R. D. Shannon and A. W. Sleight, Inorg. Chem. **7**, 1649 (1968).
[16] Y. Sato, S. Makiyama, Y. Sakamoto, T. Hasuo, Y. Inagaki, T. Fujiwara, H. S. Suzuki, K. Matsubayashi, Y. Uwatoko, and T. Kawae, Jpn. J. Appl. Phys. **52**, 106702 (2013).
[17] Y. Tabira, R. L. Withers, L. Minervini, and R. W. Grimes, J. Solid State Chem. **153**, 16 (2000).
[18] B. J. Kennedy, B. A. Hunter, and C. J. Howard, J. Solid State Chem. **130**, 58 (1997).
[19] S. T. Bramwell, M. N. Field, M. J. Harris, and I. P. Parkin, J. Phys.: Condens. Matter **12**, 483 (2000).
[20] S. S. Sosin, L. A. Prozorova, M. R. Lees, G. Balakrishnan, and O. A. Petrenko, Phys. Rev. B **82**, 094428 (2010).